The effect of Zn metal on the linear and nonlinear optical properties of Organic Phthalocyanine (Pc) material-Electrical characterization

M. Benhaliliba (mbenhaliliba@gmail.com)

Université des Sciences et de la Technologie d'Oran Mohamed Boudiaf: Universite des Sciences et de la Technologie d'Oran Mohamed Boudiaf

Research Article

Keywords: Hyperpolarizability, Nonlinear properties, DOS, MEP, HOMO-LUMO, Optical filter, Electrical parameters

Posted Date: April 12th, 2022

DOI: https://doi.org/10.21203/rs.3.rs-1335530/v1

The effect of Zn metal on the linear and nonlinear optical properties of Organic Phthalocyanine (Pc) material-Electrical characterization

[1]A. Ben Ahmed, [2,3]M. Benhaliliba, [4]Y. S. Ocak, [5]A. Ayeshamariam and [3]C.E. Benouis

[1]*University of Sfax, Faculty of Sciences of Sfax, Department of Physic, Laboratory of Applied Physic, B.P. N°802, 3018 Sfax-Tunisia*
[2]*Film Device Fabrication-Characterization and Application FDFCA Research Group USTOMB, 31130, Oran, Algeria.*
[3]*Physics Faculty, USTOMB University POBOX 1505 31130, Mnaouer Oran Algeria.*
4 Smart–Lab, 21280 Diyarbakir, Turkey.
[5]*Department of Physics, Khadir Mohideen College, Adirampattinam – 614701, Thanjavur District, Tamil Nadu, India*

Corresponding author

mbenhaliliba@gmail.com

Abstract

Organic Phthalocyanine (Pc) material is studied when Zn cation is inserted in such molecule. Effect of zinc cation on nonlinear optical properties is evidenced. Experimental Raman spectrum and theoretical spectrum of ZnPc cluster using DFT method are investigated. Absorbance profile of Phtalocyanine (Pc) and Zincphthalocynanine (ZnPc) using TDDFT approximation technique and experimental are compared. The density of states DOS are plotted and LUMO- HOMO energies are found to be -2.28 and -7.41 eV for Pc and -2.28 and -6.08 eV for ZnPc. High transparency of ZnPc film is observed within visible band and optical band gap of 3.83 eV is determined. Evaluated at 1.4 eV Urbach energy of ZnPc is then determined. A (213)-oriented monoclinic crystalline structure of ZnPc thin film is observed by X-ray pattern. A selective wavelength of 360 nm is recorded and filter optical properties are confirmed. High rectifying behavior of ZnPc/Si/Al is demonstrated and SCLC conduction mechanism is dominant inside the organic device.

Keywords. Hyperpolarizability; Nonlinear properties; DOS; MEP; HOMO-LUMO; Optical filter; Electrical parameters

1. Introduction

Phthalocyanine (Pc) comprises an electron-rich macrocycle that facilitates the substitution of different groups and coordinates many metal ions to the center of the macroring, resulting in significant effects on the chemical and physical properties of phthalocyanines (Senoglu et al. 2020; Gunay et al. 2018; Yilmaz et al. 2009; Bekaroglu et al.

1996; Ozer et al. 2006). This molecule houses macroring containing 20 π electronic systems linked together by four bridges and has a face-to-face structure that significantly affects their behaviors (Ozer et al. 2009; Koçyigit et al. 2017; Ozer et al. 2007; Koç et al. 2009). Bead-like phthalocyanine exhibits interesting properties in various applications such as nonlinear optics, gas sensors, and catalysis (Ozdag et al. 2010; Bekaroglu et al. 2010; Ceyhan et al. 2008; Saydam et al. 2009; Çimen et al. 2014; Kaki et al. 2015; Altindal et al. 2014; Ozen et al. 2016; Dogan et al. 2016). For well-defined purposes, studies on the nonlinear optical properties (NLO) of materials for optical limiting have focused on new organic materials to protect sensitive photonic devices from laser damage due to exposure to light high-intensity laser light (Liaros et al. 2013). It is, therefore, possible to enrich the nonlinear response and the optical limiting performance of the Pc molecule and their derivatives if one thinks of the adjustment of the factors affecting their nonlinear behavior such as the identity of the metal ion inserted, and modification of the symmetry of the macrocycle (Maya et al. 2000; De La Torre et al. 2004; Hann and Bloor 1989; Farajzadeh et al. 2020). In this article, we report Raman spectroscopy and UV-visible absorption experiments. The quantum chemical method (DFT and TD-DFT) was used to study vibrational activity, molecular electrostatic potential, second hyperpolarizability, electronic spectra, and energy gap analysis.

2. Experimental section

2.1. ZnPc optical properties

Spectroscopic measurements were used to identify the functional groups and to gain more information on the molecular structure. The Raman spectrum was recorded at room temperature from $100 - 2000\ cm^{-1}$ using a "Horiba-Jobin Yvon/HR800", Raman spectrometer. The optical absorption spectrum was deduced from direct transmission measurement performed, on a thin film of the material, using a spectrophotometer (SHIMADZU UV-3100) in the wavelength range $200 - 1000\ nm$.

2.2. Organic device fabrication

The chemical formula of Zinc phthalocyanine monoclinic is $C_{32}H_{16}N_8Zn$. The organic heterojunction diode is made out of ZnPc, an organic material. The Au/ZnPc/p-Si/Al organic heterojunction diode was manufactured using a vacuum NVBJ-300 NANOVAK thermal evaporation system, which was made at home. To eliminate organic contamination, a p-type Si substrate with (100) crystal orientation is first rinsed in $5H_2SO_4 + H_2O_2 + H_2O$ solution for 60 seconds before being cleaned with H_2O + HCl solution. After that, the substrate is washed

in deionized water and nitrogen dried (N2). 20 m g of both ZnPc powder supplied by Sigma-Aldrich are thermally vaporized in vacuum at low pressure once the ohmic contact is formed. A shadow mask with a diameter of 1.5 mm is used to evaporate gold metal on a ZnPc layer as a front contact. The evaporation takes place in the NVBJ-300 NANOVAK® vacuum thermal evaporation system's chamber. Fig. 12 (a) shows the cross sectional area of an Au/MPc/p-Si/Al heterojunction diode after manufacturing. The current–voltage (I–V) measurement of Au/MPc/p-Si/Al heterojunction diode is conducted in the dark using a Keithely 2400 sourcemeter from within the -3V, +3 V bias voltage range at room temperature.

3. Computational details

Optimizations in the gas phase were carried out by Gaussian09 (Frish et al. 2009), and Gaussview 5.0 (Dennington et al. 2008) was used to visualize UV-Visible spectrum and orbitals of the investigated molecules. Ground state calculations were carried out with DFT/CAM-B3LYP functional (Kohn and Sham 1965; Becke 1988; Frish 1993; Lee et al. 1988; Yanai et al. 2004) was used for optimizations and was used for obtaining UV-vis spectra in combination with the 6-31G(d,p) basis sets (Dunning and Hay 1977). Optimized structures were characterized as true minima without any imaginary frequencies. The excited states of each system were considered in the TD-DFT calculations. Molecular orbital energies and UV-vis spectra were obtained using optimized ground state geometries.

4. Results and discussions

4.1. Optimized geometry and Vibrational spectra analysis

All the physical properties of such material have their origin in the electronic structure. To have an idea of this structure, on the distribution of the charges as well as their influences on the optical and vibrational behavior of our compound, we optimized the geometry of the organic molecule (Pc) and that of the cluster (Zn-Pc). The optimized geometries are shown in Fig.1. A few bond parameters calculated for the isolated Pc molecule and the cluster compound are shown in Table 1.

The variations in the bond lengths or bond angles, particularly around the Zn-N and C-N bonds, influence the charge distribution within the ring and in turn dictate several physical characteristics. All the bond lengths and bond angles that bring the zinc connected with the nitrogen atom into play are approximately unchanged since their atoms are under the effect of the active forces from all sides by atoms of the same type (nitrogen atom) and therefore even

the order of magnitude of the attractive force. As can be seen in Table 1, the variation of the linear and angular parameters between the Pc molecule and the Zn-Pc cluster does not exceed 5.26 % and 3.30 % respectively. The variation is noted for the distances highlighting the pyrrole ring nitrogen atom (N2, N4, N6, N8), this is explained by the effect of the Zinc atom on the charge distribution in the cluster as well as the attractive force involved on the four nitrogen atoms of the pyrrole cycle. This confirms the stability of our compound.

The vibrations of the Zn-Pc compound are analyzed experimentally using Raman spectroscopy and theoretically using CAM-B3LYP/631G(d,p) method (Fig.2), getting the vibrations of the pyrrole ring along with the connecting nitrogen atoms (N2, N4, N6, N8) and the benzene ring.

To gain more information on the stability of the Pc molecule and the effects of metal at the vibrational modes, we have undertaken a vibrational study of the Pc molecule using the DFT method. The Raman spectra of the Zn-Pc cluster (experimental and theoretical) and Pc molecule (theoretical) are shown in Fig.2. We first notice the good fit between the experimental and simulated spectra for both Raman futures. Secondly, the observed and calculated vibrational frequencies along with an assignment tentative are tabulated in Table 2.

In the recorded Raman spectra, the peak at $1720\ cm^{-1}$, and $1665\ cm^{-1}$ in molecule Pc are due to the C=N, and C=C bending. In the ZnPc cluster, the intensity of these two peaks has been weakened under the effect of the Zinc atom. The strong ν(C-N-C) asymmetric stretching is represented by the peak at $1508\ cm^{-1}$ ($1528\ cm^{-1}$ and $1480\ cm^{-1}$ in the cluster and molecule Pc respectively). The corresponding C-N-C symmetric stretching is positioned at $(1447 - 1431)\ cm^{-1}$ ($1429\ cm^{-1}$ in the cluster). As can be seen in the Raman spectra of ZnPc the weak (N-Zn-N) rocking is represented by the peak at $1106\ cm^{-1}$ ($1124\ cm^{-1}$). This peak is absent in the spectrum of the isolated molecule. As can be seen in Table 2, the difference, in the frequency of vibration, between the Pc isolated molecule and those of the ZnPc cluster reaches up to 48 cm^{-1}. This is explained by the effect of the force constant imposed by the metal on the nitrogen atoms of the pyrrole cycle. A detailed assignment of the observed bands is given in Table 2.

4.2. Molecular electrostatic potential

The electrostatic potential with respect to the surface at constant electron density was mapped (Fig.3). The MEP study allows us to recognize the electrophilic and nucleophilic attack reactive sites for the project compound of study. From MEP analysis, electrophilic and nucleophilic reactivity is recognized by negative regions (red and yellow) and positive regions (blue) respectively. Inspection in Fig.3 shows the reactive sites of carbon, zinc, and nitrogen

atoms highlighting the types of attacks that occur in the system. The negative region covered under the carbon atom of a benzene ring and the maximum positive region on the Zn atom in the cluster clearly indicates a possible site of nucleophilic attack. The electrostatic potential of the nitrogen atoms when the Pc molecule is isolated is less negative compared to these same atoms during the insertion of the metal ion. Also in Fig.3, it can be seen that there is less red color grading in the area around the benzene ring carbon atoms in isolated Pc than their states when in the cluster. Compared to other nitrogen atoms, nitrogen atoms (N2, N4, N6, N8) have a less positive charge with less blue color calibration. This could be an indication of a preferential intramolecular nitrogen bond between (N2, N4, N6, N8) and Zn. This color gradation from the MEP study is useful for identifying the occurrence of an intramolecular bond. We also perceive the possibility of a donor-acceptor type interaction between the Zn atom and the nitrogen atoms (N2, N4, N6, N8).

4.3. Optical properties

4.3.1. UV-Visible spectra

The UV-Visible absorption spectrum of Zn-Pc of the spin-coated film was recorded in a range of $200-1000\,nm$ (Fig.4). As can be seen, the experimental UV-Visible spectrum of Zn-Pc shows two strong absorption regions, one in the UV region at about $200-380\,nm$ and the other in the visible region at $500-800\,nm$.

The theoretical absorption spectra, electronic transition wavelengths, and oscillator strengths of the Pc molecule, and Zn-Pc cluster were calculated by the TDDFT method. Obtained results are summarized along with the experimental ones in Table 3.

For the Zn-Pc cluster, the spectrum is mainly formed by two distinct absorption bands centered at $588\,nm$ $(2.11\,eV)$, and $300\,nm$ $(4.13\,eV)$. The first band centered at $588\,nm$ should be assigned to the charge transferred from the pyrrole ring to nitrogen atoms connected by the zinc atom. The strong band centered at $300\,nm$ should be attributed to $\pi\rightarrow\pi^*$ transitions in the pyrrole ring, and the benzene ring.

For the Pc molecule, the spectrum is mainly formed by four distinct absorption bands centered at $388\,nm$ $(3.19\,eV)$, $348\,nm$ $(3.56\,eV)$, $318\,nm$ $(3.90\,eV)$, and $295\,nm$ $(4.20\,eV)$. The first and the second bands centered at $388\,nm$ and $348\,nm$, respectively should be assigned to the charge transferred from the pyrrole ring to nitrogen atoms. The strong band centered at $295\,nm$ should be attributed to $\pi\rightarrow\pi^*$ transitions in the pyrrole ring. While the average absorption band centered at $279\,nm$ and $244\,nm$ must be attributed to $n\rightarrow\pi^*$ transitions in

the benzene ring. All the calculated electronic transitions are in very good agreement with the experimental findings.

4.3.2. The density of states (DOS) and HOMO-LUMO analysis

The FMO energies of the Zn-Pc cluster and of the Pc molecule were calculated with the TDDFT/CAM-B3LYP/6-31G(d,p) method. The HOMO-LUMO transition can be easily understood from the visualization of the orbital charge distribution on the molecules which are shown in Fig.5 and Fig.6.

The interaction between Pc and Zn was confirmed by the density of states (DOS) analysis given in Figs. 5 and 6. A considerable change in the values of E_g was observed after the insertion of the Zn atom. By comparing the heights of the peaks, it was possible to visualize that a greater number of states were available for occupancy, indicating favorable connectivity of the metal with the Pc molecule. The result obtained showed that after the interaction of the Zn metal with the Pc molecule, a considerable decrease in E_g occurred, which shifted the behavior of the dielectric to a semiconductor. It can be visualized from the DOS analysis given in Figs. 5 and 6 that the main contribution to the HOMO was due to the Zn metal and the value of the LUMO was the same for the ZnPc cluster and the isolated Pc as it contributes to the adsorption process through the HOMO orbit. By comparing the HOMO value (-7.41 eV) of the isolated Pc molecule with that of the cluster (-6.08 eV), it can be estimated that the Zn metal has strongly contributed to the adsorption process, and therefore it is resulted in an effective electrochemical sensor. As can be seen in Fig. 5, the band gap of the isolated molecule (Pc) is 5.13 eV, while the Zn-Pc cluster band gap has been reduced to 3.80 eV. The donor zinc atom provides additional carriers which cause the Fermi level to shift towards the conduction band. Therefore, the width of the bandgap decreases.

4.3.3. Urbach energy

Looking at Fig.7, it can be seen that there is a fundamental absorption edge in the 380-540 nm wavelength range. At a wavelength $\lambda < 800\ nm$, the transmissivity values decrease. The presence of such bands recommends this film as a good bandpass or optical notch filter material, depending on the wavelength. At a wavelength $\lambda > 800\ nm$, $T(\lambda)$ its value tends towards unity, the film is therefore transparent. Fig. 8 (a) shows the α versus $h\nu$ plots obtained for the ZnPc thin film sample. This plot can be divided into three regions for analysis. The first region belongs to the weak absorption (WAT-Region). It represents the

transitions that take place from a tail state located above the valence band to another tail state located below the conduction band, and/or from a tail state located below the conduction band to another tail state located above the valence band. In this WAT region, α follows $h\nu$ according to the following relationship (Singh 2006):

$$\alpha(h\nu) = \alpha_0 e^{\left(\frac{h\nu}{E_{WAT}}\right)} \quad (1)$$

Where α_0 is a constant, $h\nu$ is the photon energy and E_{WAT} represents the weak absorption tail energy.

The Urbach region (U region) (Fig. 8 (a)) represents the electronic transitions that take place from an extended valence band state to another tail state below the conduction band and/or d from a conduction band state extended to another tail state above the valence band. The E_u can be calculated by the following equation (Singh 2006):

$$\alpha(h\nu) = \alpha_0 e^{\left(\frac{h\nu}{E_u}\right)} \quad (2)$$

Where α_0 is a constant, $h\nu$ is the photon energy and E_u is the Urbach energy.

In Fig.8 (b) we have the Urbach energy ($E_u = 1.40\ eV$) this indicates that the width of the localized states in the bandgap of ZnPc thin film is due to the cumulative effect of impurities and the interactions of the excitation with the network in the system. Thus, the Tauc region (T region) in Fig. 8 (a) represents the transitions that take place between the extended valence band state and the extended conduction band state across the bandgap. Generally, two types of transitions can take place at this fundamental edge: direct and indirect transitions. In light of this, the shape of the absorption coefficient α can be described by the relation (Singh 2006):

$$(\alpha h\nu)^{1/n} \sim A\left(h\nu - E_g\right) \quad (3)$$

Where, E_g is the optical band gap, A is a proportionality constant and n takes different values corresponding to different transitions. For direct bandgap, we take $n = 2$ and for indirect bandgap, we take $n = 1/2$.

Fig.8 (c,d) shows the Tauc plot obtained for the ZnPc thin film sample. It was obtained from the T region in Fig.8 (a) as it represents the longest transition. For the ZnPc thin film sample, ZnPc, $E_g^{dir} = 3.839\ eV$ (Fig.8 (c)) for direct transition, and $E_g^{indir} = 3.811\ eV$ (Fig.8 (d)) for indirect transition. The two values are close, this indicates that the two types of transition each have a major participation in the response of ZnPc under excitation.

4.3.4. Nonlinear optical properties

The nonlinear optical materials have the advantage that when they interact with radiation, they can produce second and third harmonic effects. The interaction of the induced polarization with the applied electric field results in the conversion of the radiation. In the present study, the total dipole moment, the average polarizability, and the second hyperpolarizability of the title compounds have been calculated. In order to verify the effect of the metal on the nonlinear optical properties of the cluster object of study, we calculated the parameters quoted above for the molecule Pc, and the cluster Zn-Pc. Table 4 shows the result of these properties. We analyzed these results, we note the calculated dipole moment is equal to $55.10^{-4}\ D$ (Debye), this value is very small since the zinc atom is centered in the compound which makes the barycenter of negative charges coincide with the barycenter of positive charges almost in all directions.

The results of the linear polarizability α_{tot} undergo variations due to the effects of polarization of the crystalline medium throughout the interactive process: a variation of the results is noted for all the compounds studied. The values of the average linear polarizability converge for the Pc molecule to $28.31\ (10^{-24}\ esu)$, and to $32.17\ (10^{-24}\ esu)$ for ZnPc cluster. The results indicate that the zinc atom is a major influence on the polarization of the crystalline environment contributing to a large increase in the average linear polarizability compared with the value of the Pc molecule (see Table 4).

The result of the second hyperpolarizability $\langle\gamma\rangle$ representing a nonlinear response can be seen in Table 4. The converges the average second hyperpolarizability of the Zn-Pc cluster converge to $4.73\ (10^{-36}\ esu)$, showing that the polarization effect of the addition of the Zn atom to the pc molecule causes a8.24 % increase of the value of $\langle\gamma\rangle$.

4.4. X-ray pattern analysis

The analysis of sample is carried out in room temperature within 10-100 deg. 2θ position range. Fig. 9 demonstrates the X-ray pattern of ZnPc organic molecule recording one (213) peak at 22.4 deg. 2θ position. The grain size is then determined by Scherrer formula (Meftah et al. 2021):

$$\boldsymbol{D = \frac{0.94\lambda}{\beta \cos\theta}} \qquad (4)$$

The grain size of ZnPc is evaluated at 7.60 Å and the lattice parameters of ZnPc lattice are a=14.52 Å, b=4.87 Å, c=17.22 Å, β= 106.15° determined by (El-Nahasset al. 2004 And Tombak et al. 2015):

$$\frac{1}{d_{hkl}^2} = \frac{h^2}{a^2 sin^2\beta} + \frac{k^2}{b^2} + \frac{l^2}{c^2 sin^2\beta} - \frac{2hl\ cos\beta}{ac\ sin^2\beta} \quad (5)$$

The XRD study yielded values in the range of 7.6-11.58, validating the nanostructural aspect. Such obtained data reveal that the ZnPc and MgPc films have smaller grit sizes when viewed in the directions (213) and (123), respectively, whereas the AlPc-Cl film has a greater size when viewed in the direction (242).

4.5. Optical filter properties

Fig.10 demonstrates the peak and valley of transmittance vs. photon wavelength as indicated by stars. The range of transmittance within 30-50 % range as showed by dotted circle and displayed in the inset of Fig 10. The narrowed range of photon wavelength is of 360 nm comprises the peak F1 and valley F2 are separated by 161 nm, which are related to 479 nm ($5.89x10^{14}$ Hz) and 695 nm ($4.47x10^{14}$ Hz) respectively. This behavior reveals the optical filter properties of ZnPc organic thin layer which selects this narrowed of wavelength. Our device's transmittance curve has a peak and valley that could operate as an optical filter.
The derivative of transmittance plot versus photon wavelength of ZnPc layer. The peak shows the wavelength 405.19 nm and optical band gap E_g=3.06 eV as shown in Fig 10a. Various values of Eg metal-phthalocyanine materials are reported like 2.94 eV for as-grown ZnPc, 2.88 eV for annealed ZnPc, 2.63 eV for FePc, 2.6 eV for MgPc and 2.42 eV for PbPc (El-Nahass et al. 2004).

Transmittance-Absorbance plot versus photon wavelength of ZnPc organic thin film describe a quasi-symmetric shape within UV-Vis-IR spectrum bands as portrayed in Fig.11. As shaped in dashed rectangle, the 1st peak corresponding to absorbance inside UV range is highly shaped (98%), the lesser intensity peaks (80%) of both transmittance and absorbance are included in VIS rectangle as depicted in Fig.11. Beyond 800 nm the curve of transmittance increases to around 80% within IR band while absorbance is lowering to 20%. The absorption spectra of NiPc 400 nm thick layer is reported by El-Nahass (El-Nahass et al. 2005).

The spectral distribution of transmittance and reflectance R of different thickness for as-deposited and annealed MgPc thin films describe similar tendency of peak and valley presence (El-Nahass et al. 2008).

The intensity of the peak at 620 nm increases quicker than the peak at 691 nm as the thickness of electrodeposited CuPc increases as reported prior (Rajaputra et al. 2009). The peak at 620 nm is for dimer phthalocyanine, while the peak at 691 nm is for monomer phthalocyanine (He et al. 2006). This means that as CuPc thickens the percentage of dimer phthalocyanine increases.

4.6. Electrical measurement

Electrical characterization of ZnPc/Si heterojunction diode is achieved in dark and room temperature. The cross-section profile of an ZnPc/p-Si/Al heterojunction diode prepared by thermal evaporation is shown in Fig. 12a. The I-V characteristics of ZnPc/Si is achieved within -3V, 3V range showing two branches reaching 122 µA at +3V and 15.45 nA at -3V.

By using the Cheung-Cheung and Norde approximation methods (not shown here) (Missoum et al. 2016). From dV/dlnI plots, the ideality factor is of 4.8 and series resistance (Rs) is higher found to be 7.9 kΩ. While by H-I function, Rs and barrier height are of 7.9 kΩ and 0.69 eV. Norde method exhibits a value of 8.4 kΩ and 0.69 eV. High rectifying ratio (RR) of such organic device based on ZnPc of 6100 is recorded as seen in Fig.12b. Reported values of n and Rs, determined by dV/dlnI, are of 3.29 and 33Ω for MgPc/GaAs, 8.87 and 3.36Ω for MgPc/nSi and 2.4 and 1.9 kΩ for MgPc/pSi as studied before (Missoum et al. 2016). The ideality factor n, greater than the unity, expresses as (Meftah et al. 2020):

$$n = \frac{q}{kT}\frac{dV}{d(lnI)} \qquad (6)$$

To strengthen our study, the conduction mechanisms are studied inside the device based on organic ZnPc molecule.

The Cheung and Cheung approximation tool (Cheung et al. 1986) is used to calculate series resistance in order to better understand and analyse these effects.

$$\frac{dV}{d(lnI)} = IR_s + n\left(\frac{kT}{q}\right) \quad (7)$$

Voltage is expressed as a second function in terms of temperature (Cheung et al. 1986):

$$\mathbf{H(I) = V - \left(\frac{nkT}{q}\right) ln\left(\frac{I}{AA^{*}T^{2}}\right)} \quad (8)$$

As follows, a simplified equation has been reworded (Cheung et al. 1986):

$$H(I) = IR_S + n\phi_B \quad (9)$$

In order to pursue the calculation of different electrical parameters of ZnPc based organic device, Norde method is evidenced as follows. Norde approximation is another tool to assess the the series resistance, is written as (Norde et al. 1979):

$$\mathbf{F(V) = \frac{V}{\gamma} - \frac{kT}{q} ln\left(\frac{I(V)}{AA^{*}T^{2}}\right)} \quad (10)$$

Where γ is the first integer number higher than the ideality factor diode, I and V are achieved from the forward bias of $I(V)$ characteristics. The barrier height of the heterostructure expresses as (Norde et al. 1979):

$$\phi_B = F(V_0) + \frac{V_0}{\gamma} - \frac{kT}{q} \quad (11)$$

Where the minimum value $F(V_0)$ is taken from the $F(V)$ vs V plotting (not shown here), and the corresponding voltage isV_0. Moreover, R_s is determined by (Norde et al. 1979):

$$\mathbf{R_S = \frac{kT(\gamma - n)}{qI_{min}}} \quad (12)$$

Where the minimum value of the current I_{min} corresponds to the value of V_0.

By plotting the logI-logV (not shown here) within the forward voltage region, a linear segment is selected to evaluate the m exponent as a slope of curve according to I αV^{m} law within 0.11-1 V range. As mentioned earlier, the RR and Rs values of ZnPc/Si diode, are

found to be 9.42 and 9.72 MΩ respectively (Aziz 2006) Such high series resistance value is attributed to the high resistance of the ZnPc thin film (Aziz 2006).

The evaluation by linear fit yields a value of 2.7 to m which confirms the space charge limited conduction (SCLC) mechanism occurrence inside the device based on ZnPc/Si. As a result, different contacts have varying barrier heights (0.69 eV for Au/ZnPc/p-Si/Al and 0.77 eV for Ag/ZnPc/n-Si/Au), which effects charge carrier exchange at the metal/semiconductors interface. While Aziz stated that the current density has a power law dependence of the type J αV^m where m>4, indicating that SCLC mechanism is governed by an exponential trap distribution (Aziz 2006).

5. Conclusions

DFT calculations were performed to estimate the UV-vis absorption spectra and the second hyperpolarizability of the title compound. The calculated electronic transitions, HOMO-LUMO energy values, DOS spectrum, and the study of nonlinear optical properties indicate the important role of the phthalocyanine molecule which has high chemical stability and high excitation energy. The electronic structure analysis showed that after the interaction of the Zn metal with the Pc molecule, a considerable decrease in E_g occurred, which shifted the behavior of the dielectric to a semiconductor.

A peak indicating the (213) orientation of monoclinic crystalline structure of ZnPc layer is confirmed by X-ray pattern analysis. ZnPc film exhibits a high transparency of 70% within visible range at 509 nm is recorded. Selective aspect of photon wavelength of 360 nm is obtained by ZnPc organic layer. A gap of 3.06 eV is determined by dT/dλ technique. A high symmetry of transmittance-absorbance profiles demonstrating peaks and valleys followed by a slight variation of T-A within IR range. High rectifying, RR=6100, of organic diode based on ZnPc/Si is successfully fabricated by thermal evaporation technique. Such characteristics can provide to such fabricated organic device based on ZnPc material many applications like optical device applications and solar cell and microelectronic applications.

Acknowledgment

The work is included in the PRFU project under contract number B00L02UN310220220001 Oran University of sciences and technology USTO-MB. www.mesrs.dz, and www.univ-usto.dz, http://www.prfu-mesrs.dz https://www.mendeley.com/impact/mostefa-benhaliliba https://orcid.org/0000-0001-6507-3663

Conflict of Interest

The authors declare that they have no conflict of interest

References

[1] Şenoğlu, S., Özer, M., Dumludağ, F., Acar, N., Salih, B., Bekaroğlu, Ö.: Synthesis, characterization, DFT study, conductivity and effects of humidity on CO_2 sensing properties of the novel tetrakis-[2-(dibenzylamino)ethoxyl] substituted metallophthalocyanines. Sensors and Actuators B Chemical. 127860 (2020)

[2] Günay, İ., Orman, E. B., Altındal, A., Salih, B., Özer M., Özkaya, A. R.: Novel tetrakis 4-(hydroxymethyl)-2,6-dimethoxyphenoxyl substituted metallophthalocyanines: Synthesis, electrochemical redox, electrocatalytic oxygen reducing, and volatile organic compounds sensing and adsorption properties. Dyes and Pigments.154, 172-187 (2018)

[3] Yılmaz F., Özer M., Kani I., Bekaroğlu Ö.: Catalytic Activity of a Thermoregulated, Phase-Separable Pd(II)-perfluoroalkylphthalocyanine Complex in an Organic/Fluorous Biphasic System: Hydrogenation of Olefins. Catalysis letters. 130, 642-647 (2009)

[4] Bekaroğlu, Ö.: Phthalocyanines containing macrocycles. Applied organometallic chemistry. 10, 605-622 (1996)

[5] Özer, M., Altındal, A., Özkaya, A. R. Bulut, M. Bekaroğlu, Ö.: Synthesis, characterization and some properties of novel bis (pentafluorophenyl) methoxyl substituted metal free and metallophthalocyanines. Polyhedron. 25, 3593-3602 (2006)

[6] Özer, M., Altındal, A., Özkaya, A. R., Bekaroğlu, Ö.: Ball-type supramolecular metallophthalocyanines with eight perfluorodecyl units: chemosensors for SO 2 and electrocatalysts for oxygen reduction. Dalton transactions. 17, 3175-3181 (2009)

[7] Koçyiğit, N., Özen, Ü. E., Özer, M., Salih, B., Özkaya, A. R., Bekaroğlu, Ö.: Electrocatalytic activity of novel ball-type metallophthalocyanines with trifluoro methyl linkages in oxygen reduction reaction and application as Zn-air battery cathode catalyst. Electrochimica Acta. 233, 237-248 (2017)

[8] Özer, M., Altındal, A., Özkaya, A. R., Salih, B., Bulut, M., Bekaroğlu, Ö.: Synthesis, characterization, and electrochemical and electrical properties of novel pentaerythritol-bridged cofacial bismetallophthalocyanines and their water-soluble derivatives. European journal of inorganic chemistry. 2007, 3519-3526 (2007)

[9] Koç, I., Özer, M., Özkaya, A., Bekaroğlu, Ö.: Electrocatalytic activity, methanol tolerance and stability of perfluoroalkyl-substituted mononuclear, and ball-type dinuclear cobalt phthalocyanines for oxygenreduction in acidic medium. Dalton transactions. 6368-6376 (2009)

[10] Özdağ, M. A., Ceyhan, T., Ünver, H., Elmali, A., Bekaroğlu, Ö.: Strong optical limiting property of a ball-type supramolecular zinc-phthalocyanine in polymer-phthalocyanine composite film. Opt Com. 283, 330-334 (2010)

[11] Bekaroğlu, Ö.: Ball-Type Phthalocyanines: Synthesis and Properties Ozer Bekaroglu ,Structure and Bonding. Springer. 135, 105-136 (2010)

[12] Ceyhan, T., Özdağ, M. A., Salih, B., Erbil, M. K., Elmalı, A., Özkaya, A. R., Bekaroğlu, Ö.: Synthesis, Characterization, Nonlinear Absorption and Electrochromic Properties of Double-Decker Octakis (mercaptopropylisobutyl-POSS) phthalocyaninatolanthanide (III) Complexes. Europ. J. of Inorg. Chem. 31, 4943-4950 (2008)

[13] Saydam, S., Yılmaz, E., Bağcı, F., Yağlıoğlu, H. G., Elmalı, A., Salih, B., Bekaroğlu, Ö.: Synthesis, Characterization, Electrochemical, and Optic Limiting Properties of Novel Co-II, Cu-II, and Double-Decker Lu-III Phthalocyanines. Europ. J. of Inorg. Chem. 14, 2096-2103 (2009)

[14] Çimen, Y., Ermiş, E., Dumludağ, F., Özkaya, A. R., Salih, B., Bekaroğlu, Ö.: Synthesis, characterization, electrochemistry and VOC sensingproperties of novel ball-type dinuclear metallophthalocyanines. Sensors and Actuators B Chemical. 202, 1137-1147 (2014)

[15] Kakı, E., Altındal, A., Salih, B., Bekaroğlu, Ö.: Synthesis, characterization and gas sensing properties of novel homo and hetero dinuclear ball-type phthalocyanines. Dalton transactions. 44, 8293-8299 (2015)

[16] Altındal, A., Kurt, Ö., Şengül, A., Bekaroğlu, Ö.: Kinetics of CO2 adsorption on ball-type dicopper phthalocyanine thin film. Sensors and Actuators B: Chemical. 202, 373-381 (2014)

[17] Özen, Ü. E., Doğan, E., Özer, M., Bekaroğlu, Ö., Özkaya, A. R.: Communication—High-performance and non-precious bifunctional oxygen electrocatalysis with binuclear ball-

type phthalocyanine based complexes for zinc-air batteries. J. of The Electrochem. Soc. 163, A2001 (2016)

[18] Doğan, E., Özer, M., Altındal, A., Özkaya, A. R., Salih, B., Bekaroğlu, Ö.: Novel 4,4′-{(diphenylmethylene) bis(4,1-phenylene)bis(oxy)}-bridged ball-type phthalocyanines: Electrochemical, electrocatalytic oxygen reducing and heavy metals ions sensing properties. J. Porphyr. Phthalocya. 20, 1319-1333 (2016)

[19] Liaros, N., Iliopoulos, K., Stylianakis, M. Koudoumas, E., Couris, S.: Optical limiting action of few layered graphene oxide dispersed in different solvents. Opt. Mat. 36, 112-117 (2013)

[20] Maya, E. M., Garcia, C., García-Frutos, E. M., Vázquez, P., Torres, T.: Synthesis of Novel Push-Pull Unsymmetrically Substituted Alkynyl Phthalocyanines. J. of org. chem. 65, 2733-2739 (2000)

[21] De La Torre, G., Vazquez, P., Agullo-Lopez, F., Torres, T. : Role of structural factors in the nonlinear optical properties of phthalocyanines and related compounds. Chem. Rev. 104, 3723-3750 (2004)

[22] Hann, R., Bloor, D.: Organic materials for non-linear optics. Roy. Soc. of Chem. London, (1989)

[23] Farajzadeh, N., Kösoğlu, G., Erdem, M., Eryürek, G., Koçak, M. B.: Synthesis, characterization, third-order non-linear optical properties and DFT studies of novel SUBO bridged ball-type metallophthalocyanines. Synt. Met. 266, 116440 (2020)

[24] Frisch, M., Trucks, G., Schlegel, H. B., Scuseria, G. E., Robb, M. A., Cheeseman, J. R., Scalmani, G., Barone, V., Mennucci, B., Petersson, G.: Inc., Wallingford CT. 201 (2009)

[25] Dennington, R., Keith, T. A., Millam, J. M.: Inc., Wallingford. (2008)

[26] Kohn, W., Sham, L. J.: Self-Consistent Equations Including Exchange and Correlation Effects. Phys. Rev. 140, A1133 (1965)

[27] Becke, A. D.: Density-functional exchange-energy approximation with correct asymptotic behavior. Phy. Rev. A. 38, 3098 (1988)

[28] Frisch M.: Density-functional thermochemistry. III. The role of exact exchange. J. Chem. Phys. 98, 5648 (1993)

[29] Lee, C., Yang, W., Parr, R. G.: Development of the Colle-Salvetti correlation-energy formula into a functional of the electron density. Phy. Rev. B. 37, 785 (1988)

[30] Yanai, T., Tew, D. P., Handy, N. C.: A new hybrid exchange–correlation functional using the Coulomb-attenuating method (CAM-B3LYP). Chem. Phy. Lett. 393,51-57 (2004)

[31] Dunning T. H., Hay, P. J.: In Modern theoretical chemistry. Plenum Press New York. 3, 1 (1977)

[32] Singh. J.: Optical Properties of Condensed Matter and Applications. Wiley (2006)

[33] Meftah, S.E., Benhaliliba, M., Kaleli, M., Benouis, C.E., Yavru, C.A., Bayram, A.B.: Innovative Organic MEH-PPV Heterojunction Device Made by USP and PVD. J. of ELEC. MAT. https://doi.org/10.1007/s11664-021-08738-6 (2021)

[34] El-Nahass, M. M., Zeyada, H. M., Aziz, M. S., El-Ghamaz, N. A.: Structural and optical properties of thermally evaporated zinc phthalocyanine thin films. Opt. Mat. 27, 491–498, (2004)

[35] Tombak, A., Benhaliliba, M., Ocak, Y. S., Kiliçoglu, T.: The novel transparent sputtered p-type CuO thin films and Ag/p-CuO/n-Si Schottky diode applications. Results in Physics. 5 314–321, (2015).

[36] El-Nahass, M.M., Abd-El-Rahman, K.F., Darwish, A.A.A.: Fourier-transform infrared and UV–vis spectroscopes of nickel phthalocyanine thin films. Mat. Chem. and Phy. 92, 185–189 (2005)

[37] El-Nahass, M.M., Atta, A.A., El-Sayed, H.E.A., El-Zaidia, E.F.M.: Structural and optical properties of thermal evaporated magnesium phthalocyanine (MgPc) thin films. App. Surf. Sc. 254, 2458–2465 (2008)

[38] Rajaputra, S., Sagi, G., Singh, V. P. : Schottky diode solar cells on electrodeposited copper phthalocyanine films . Solar Energy Materials & Solar Cells. 93, 60– 64 (2009)

[39] He, Z., Zhao, G., Han, G.: Optical and photoelectric properties of copper phthalocyanine/cadmium sulphide multilayer films prepared by vacuum sublimation. Phys. Stat. Sol. (A). 203, 518-525 (2006)

[40] Missoum, I., Ocak, Y.S., Benhaliliba, M., Benouis, C.E., Chaker, A.: Microelectronic properties of organic Schottky diodes based on MgPc for solar cell applications. Synt. Met. 214, 76-81 (2016)

[41] Meftah, S.E., Benhaliliba, M., Kaleli, M. Benouis, C.E., Yavru, C.A., Bayram, A.B.: Optical and electrical characterization of thin film MSP heterojunction based on organic material Al/p-Si/P3HT/Ag. Physica B: Cond. Matter. 593, 412238 (2020)

[42] Cheung, S.K., Cheung, N.W.: Extraction of Schottky diode parameters from forward current-voltage characteristics. Appl. Phys. Lett. 49 85 (1986).

[43] Norde, H.: A modified forward I - V plot for Schottky diodes with high series resistance. J. Appl. Phys. 50, 5052–5053 (1979)

[44] Aziz, M.S.: Carrier transport mechanisms and photovoltaic properties of Au/p-ZnPc/Al device. Solid State Electr. 50, 1238–1243 (2006)

Figures and Tables

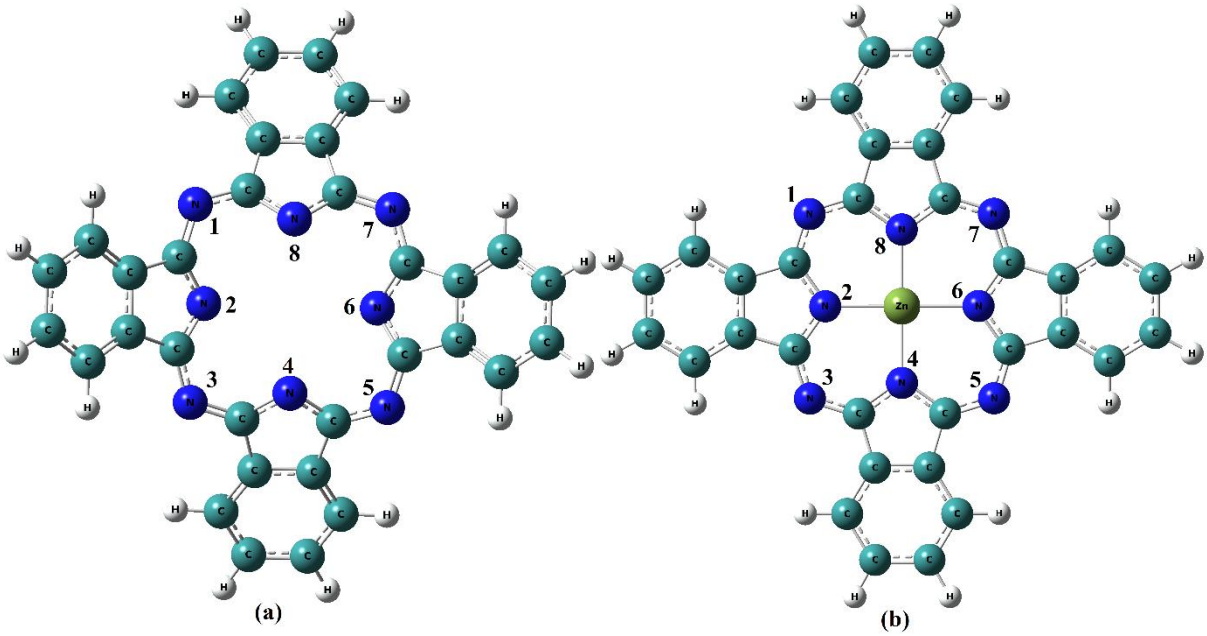

Fig.1. Optimized molecular structure of Pc (a) and Zn-Pc (b).

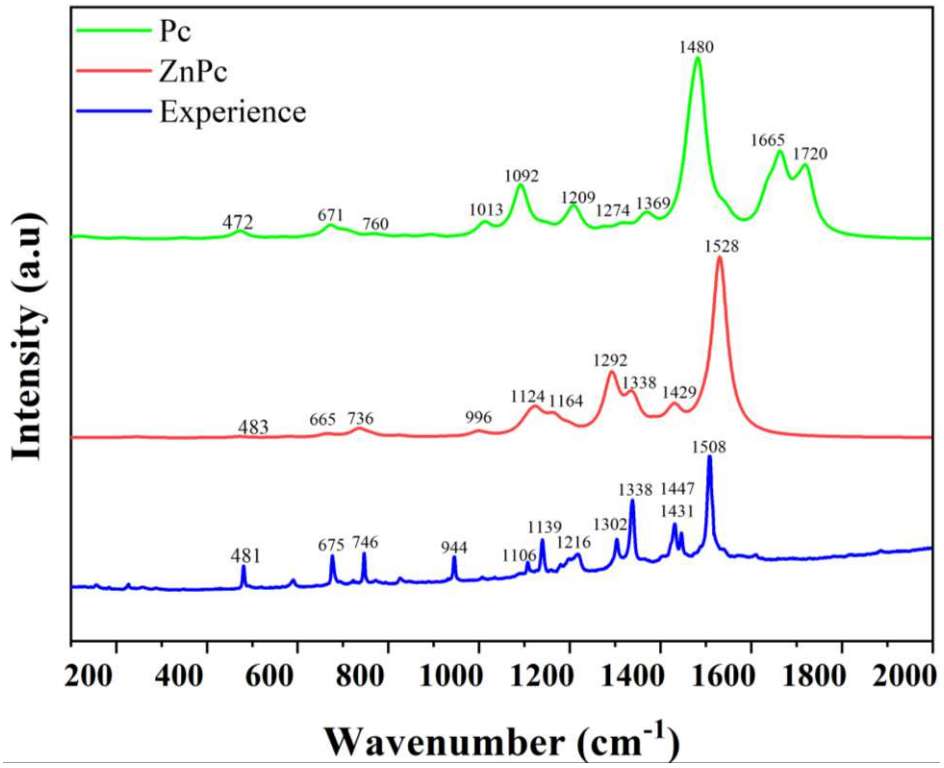

Fig.2. Experimental Raman spectrum of Zn-Pc and theoretical spectra of Zn-Pc cluster and Pc molecule computed using DFT method.

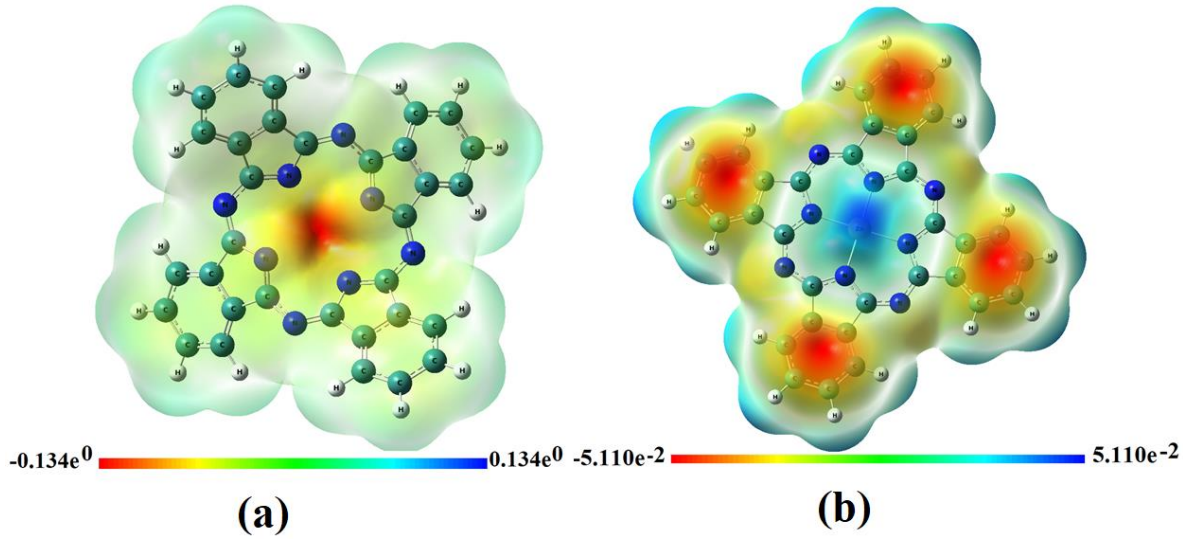

Fig.3. MEP and contour plots of Pc and Zn-Pc.

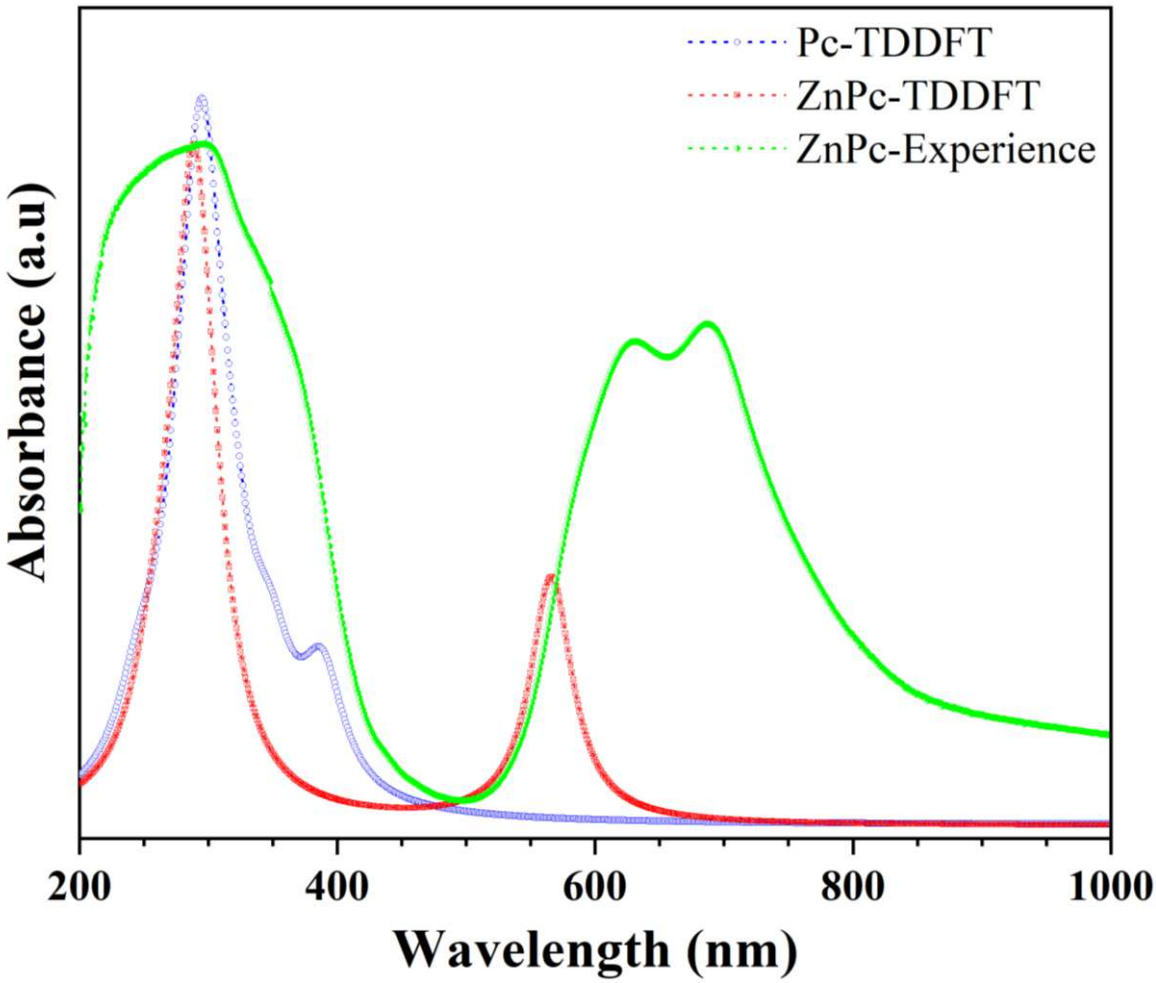

Fig.4. UV-Visible spectra of Zn-Pc cluster and Pc molecule.

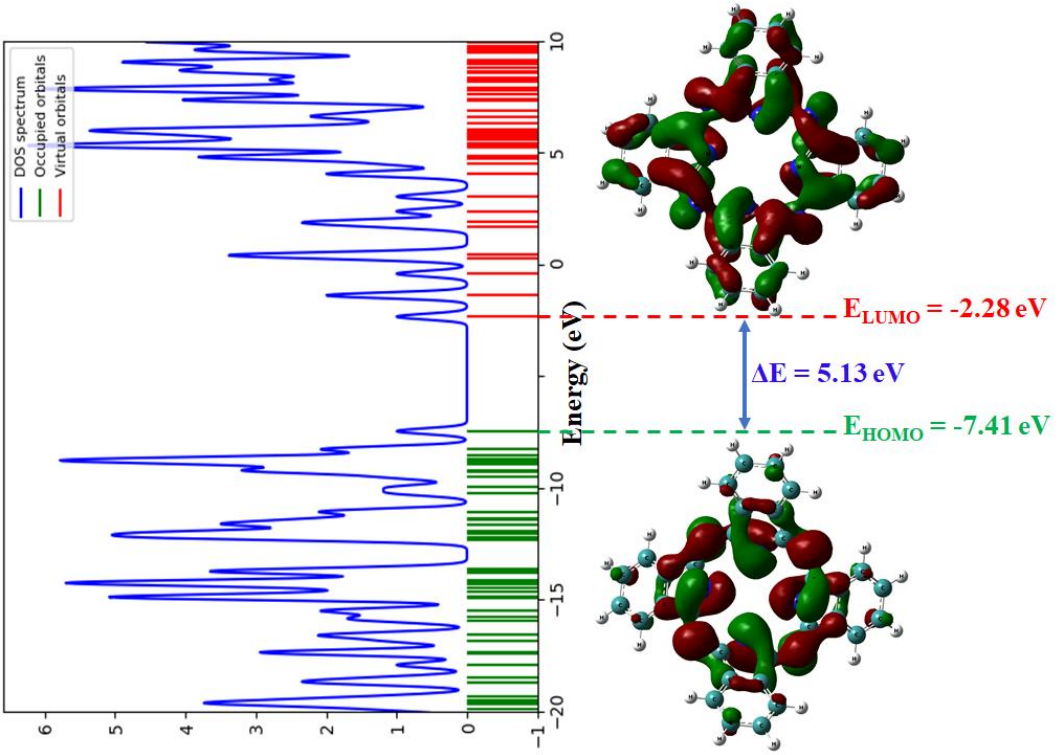

Fig.5.The molecular orbitals and DOS spectrum of the Pc molecule.

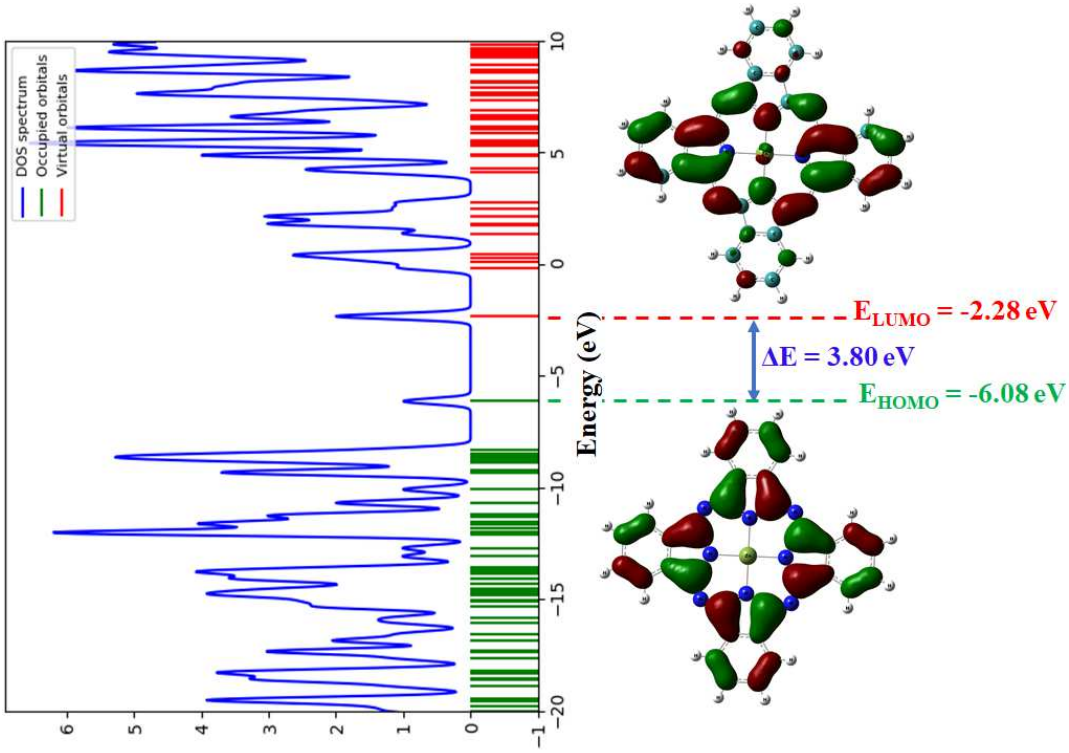

Fig.6. The molecular orbitals and DOS spectrum of the Zn-Pc.

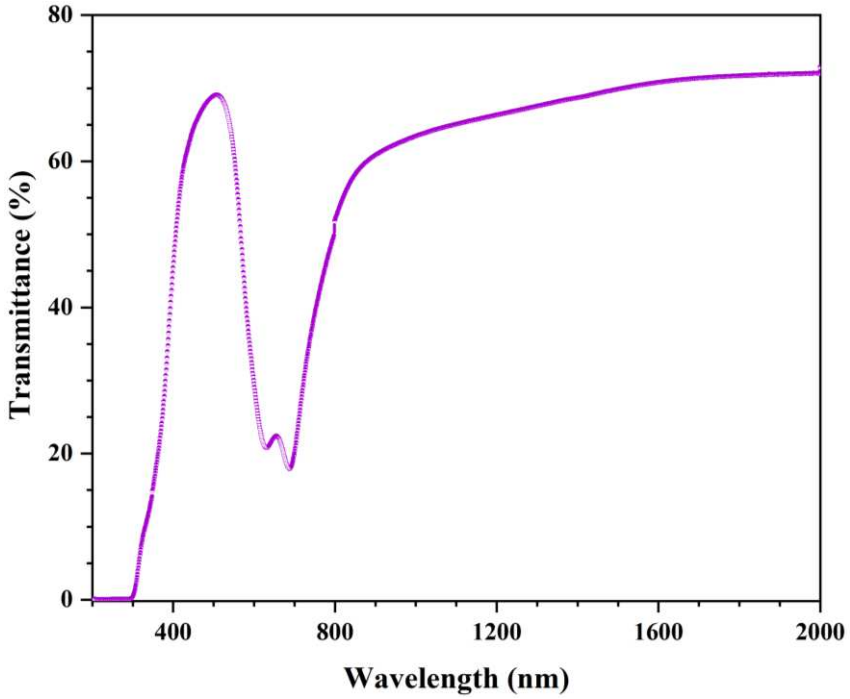

Fig.7. The spectrum of transmittance for ZnPc thin film.

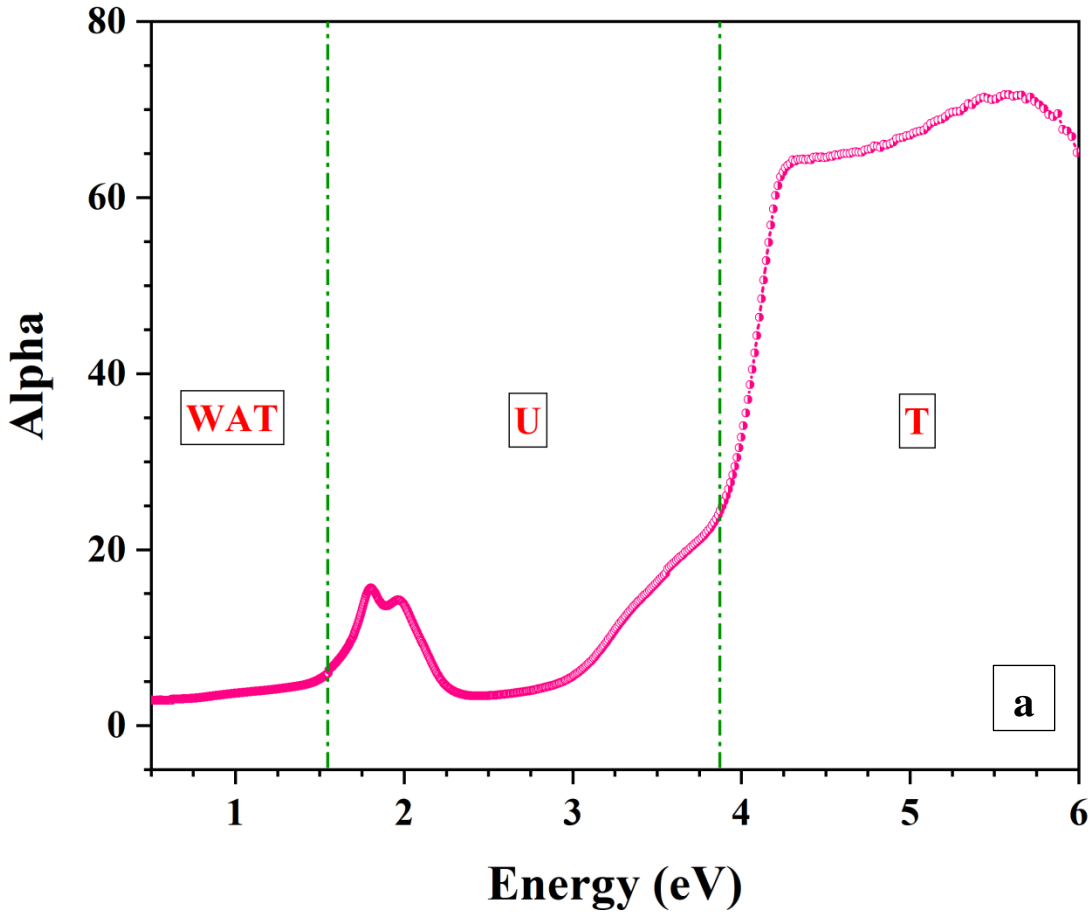

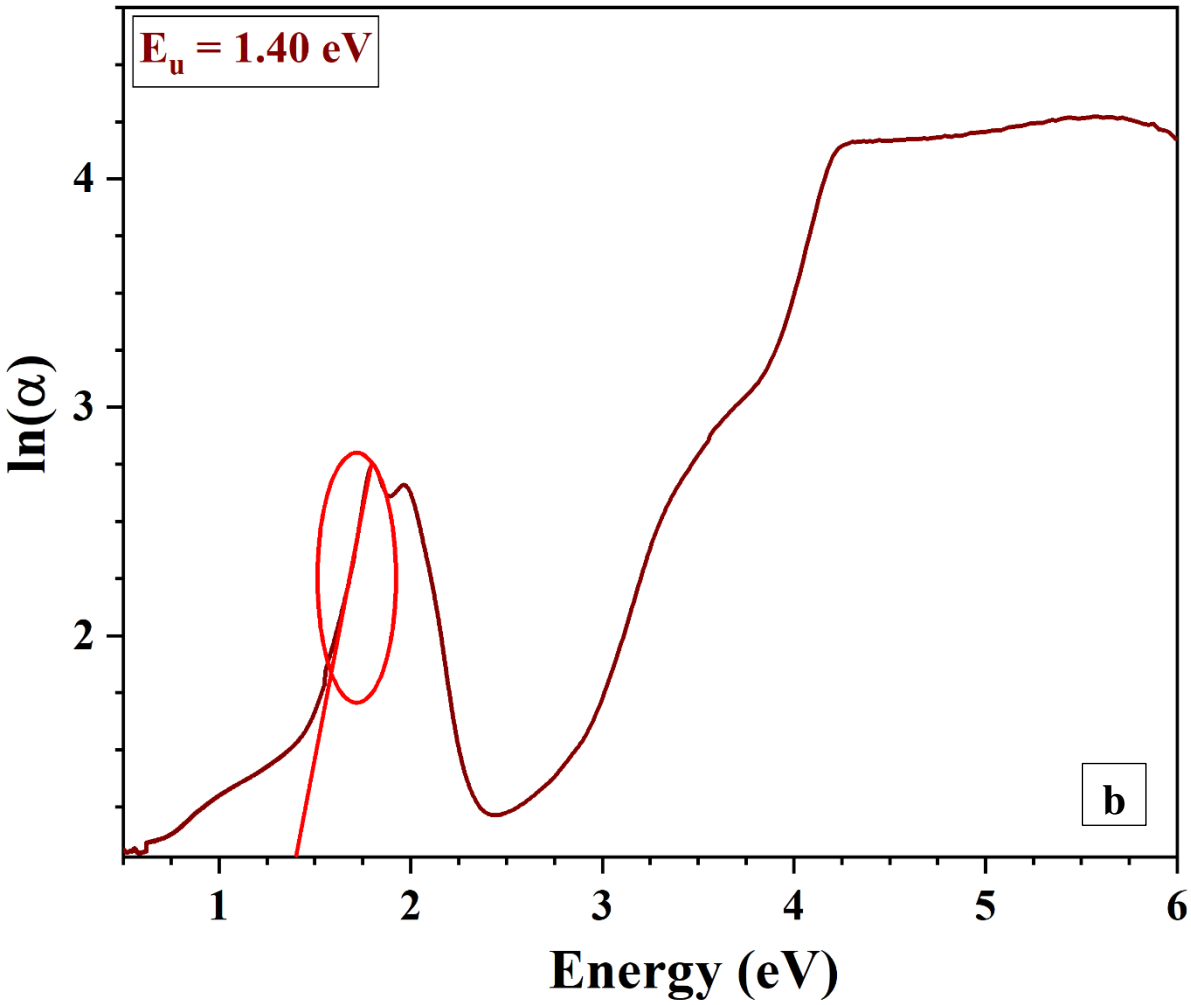
E_u = 1.40 eV
ln(α)
Energy (eV)
b
1
2
3
4
5
6
2
3
4

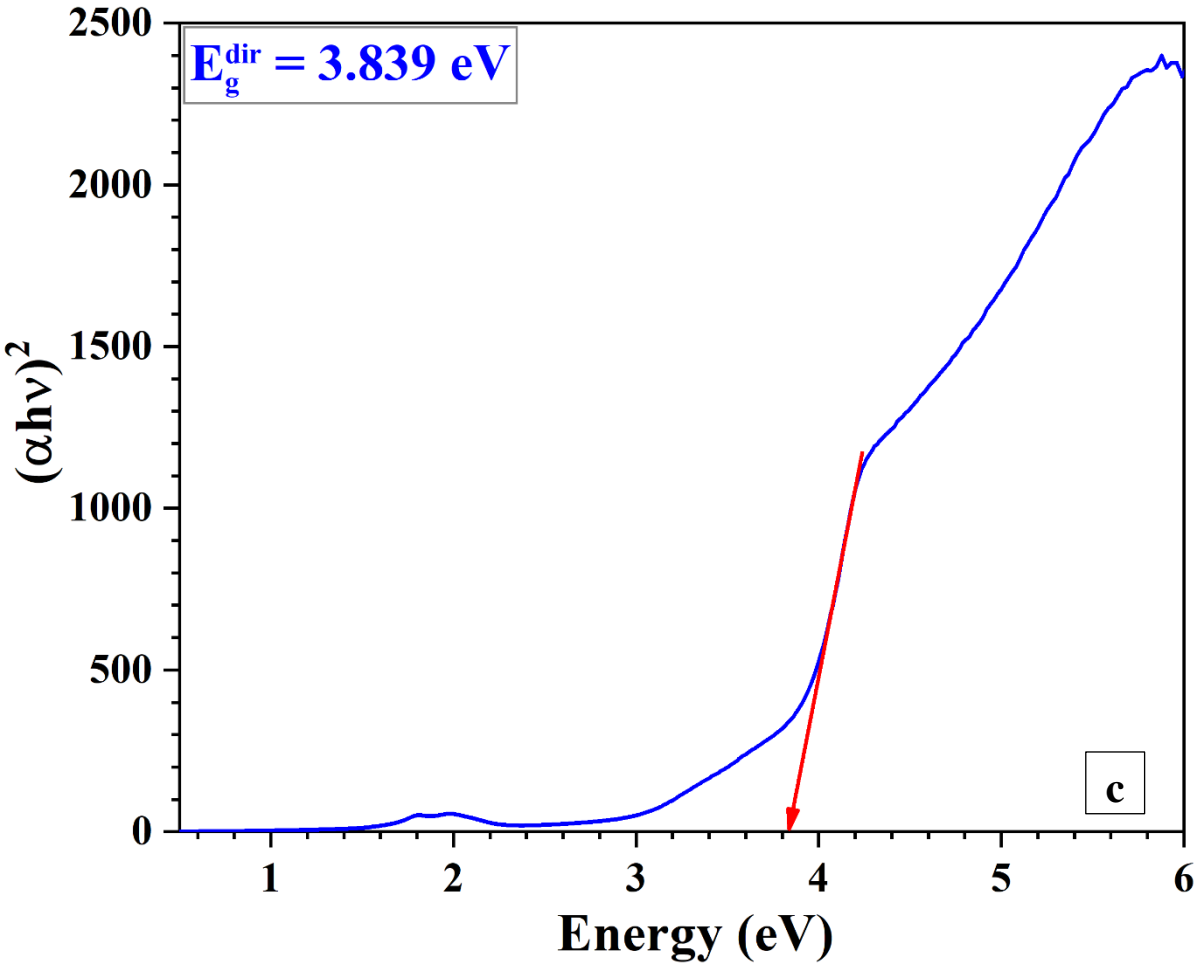
E_g^{dir} = 3.839 eV
$(\alpha h\nu)^2$
Energy (eV)
c
2500
2000
1500
1000
500
0
1
2
3
4
5
6

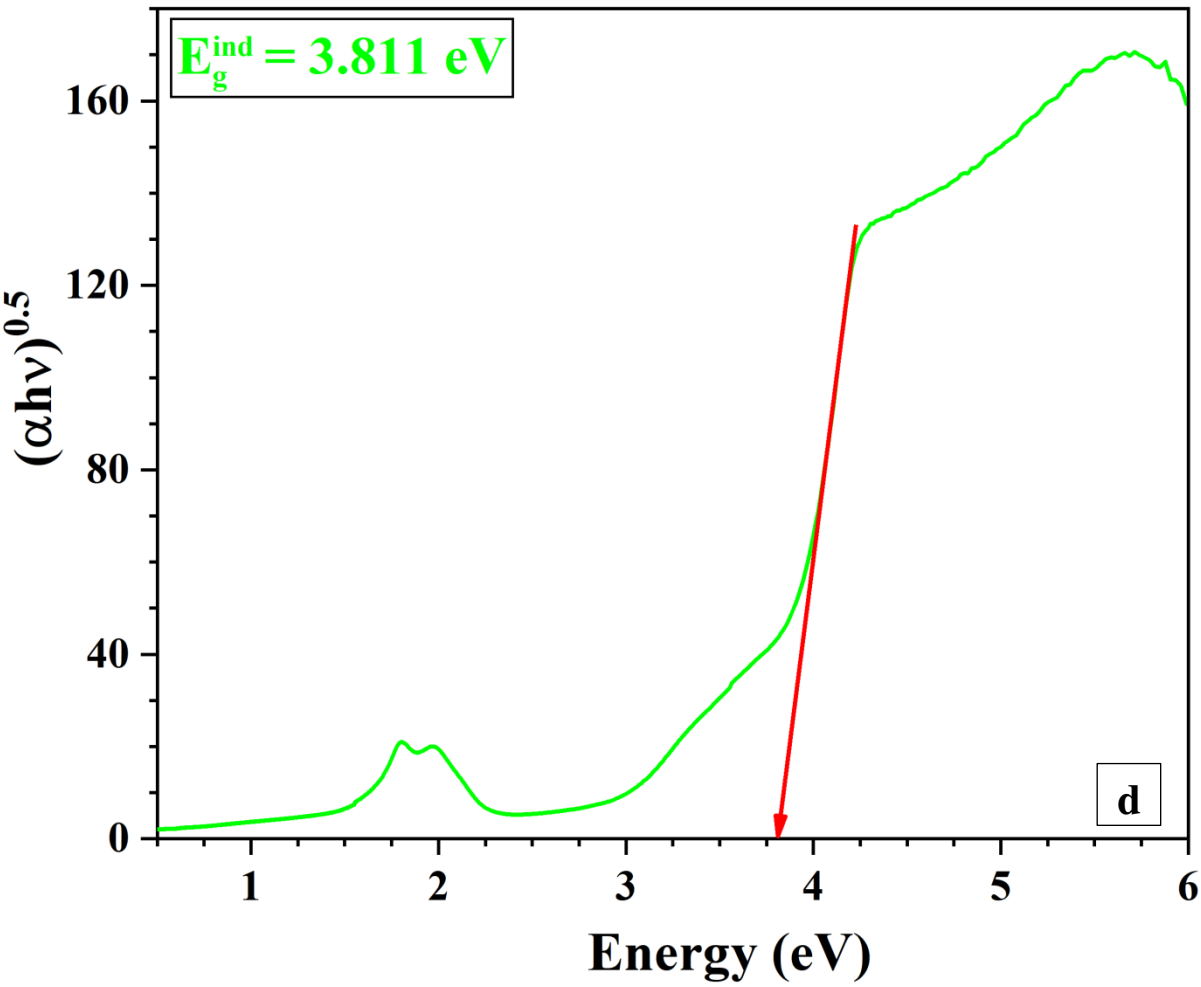

Fig.8. Variations of absorption coefficient (a), Urbach energy (b), and optical bandgap energy (c, d) with incident photon energy.

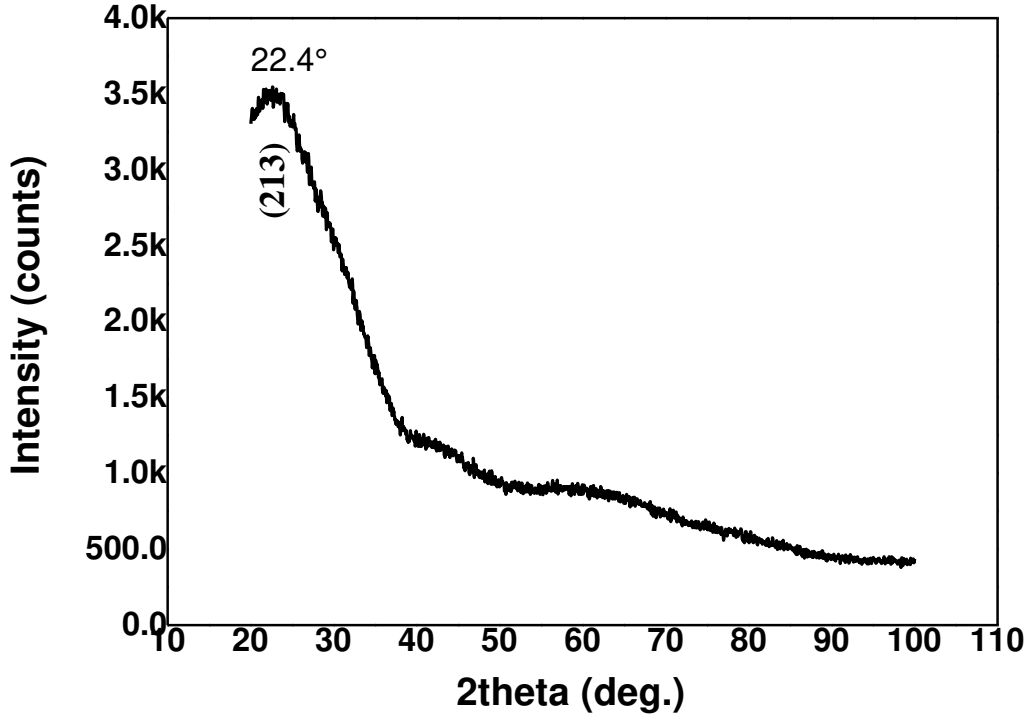

Fig.9. X-ray pattern of ZnPc organic thin layer onto glass substrate.

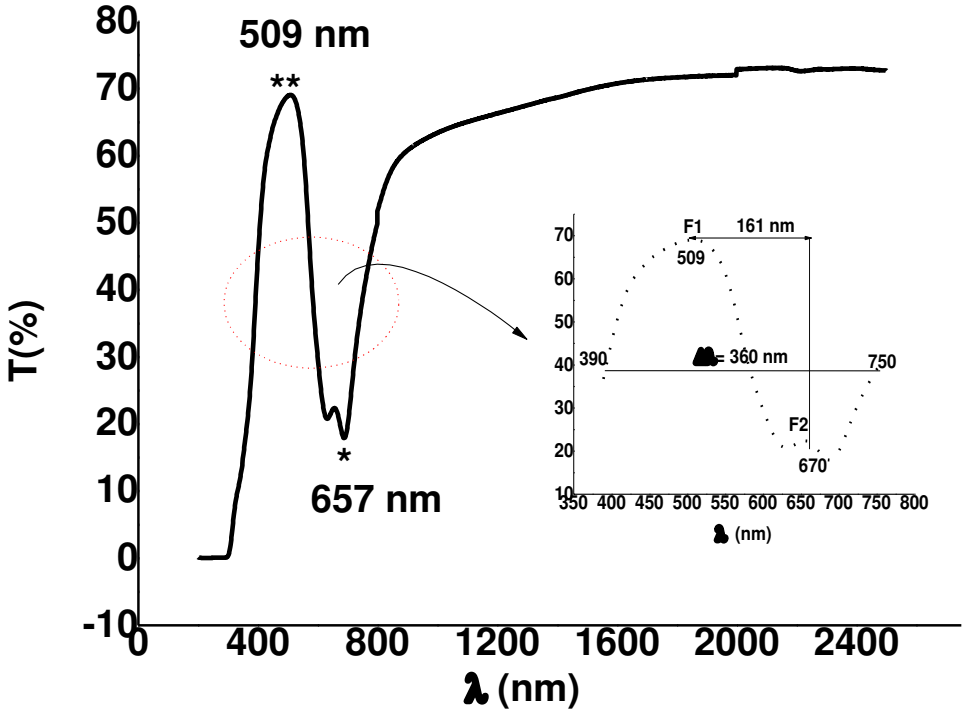

Fig. 10. The sketch of optical filter of transmittance versus photon wavelength of ZnPc layer. The inset shows the peak F1 and valley F2.

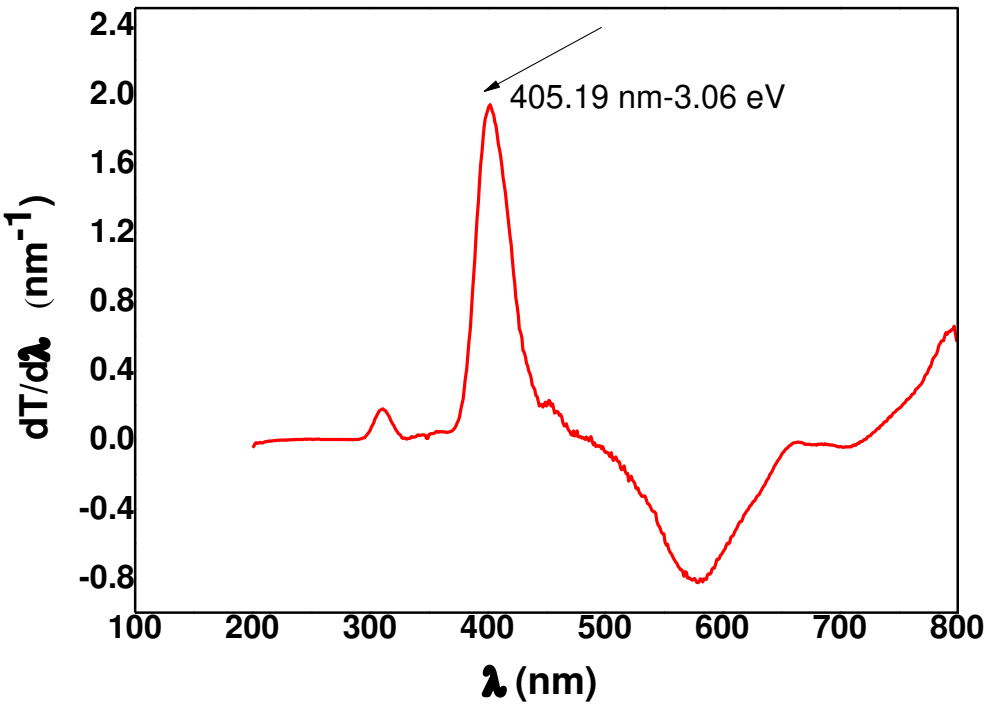

Fig. 10a. The derivative of transmittance plot versus photon wavelength of ZnPc layer. The peak shows the wavelength 405.19 nm and optical band gap Eg=3.06 eV.

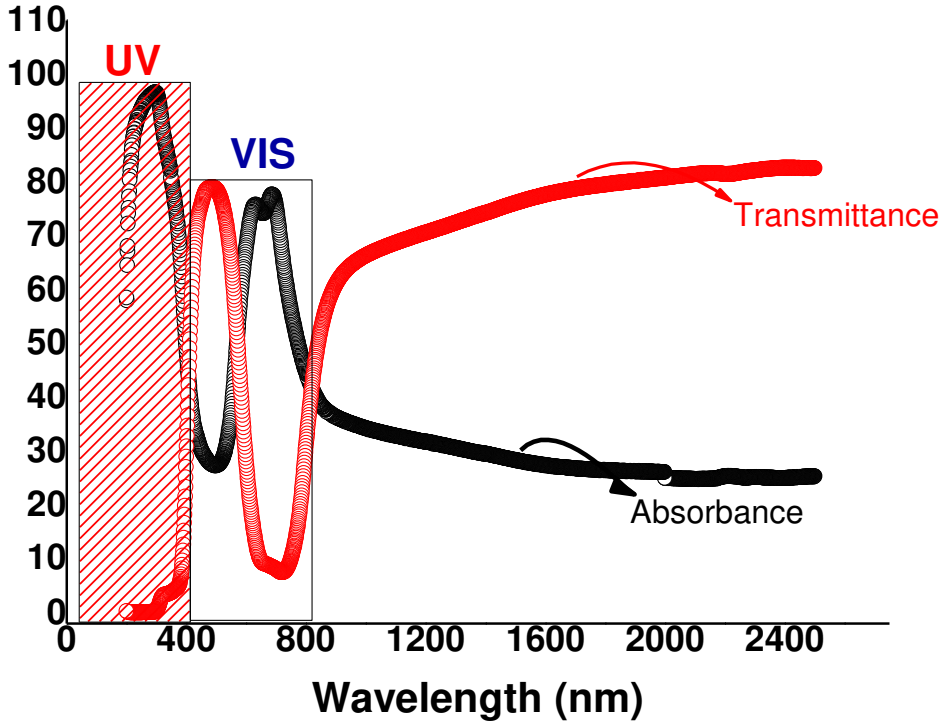

Fig. 11. Transmittance-Absorbance plot versus photon wavelength of ZnPc organic compound

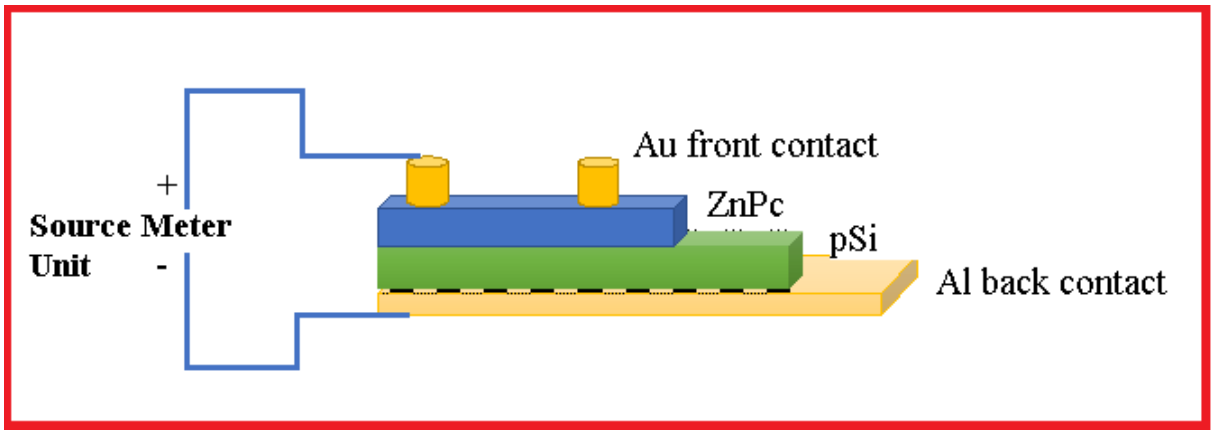

Fig. 12a. The cross section profile of ZnPc/p-Si/Al heterojunction diode shaped by thermal evaporation process.

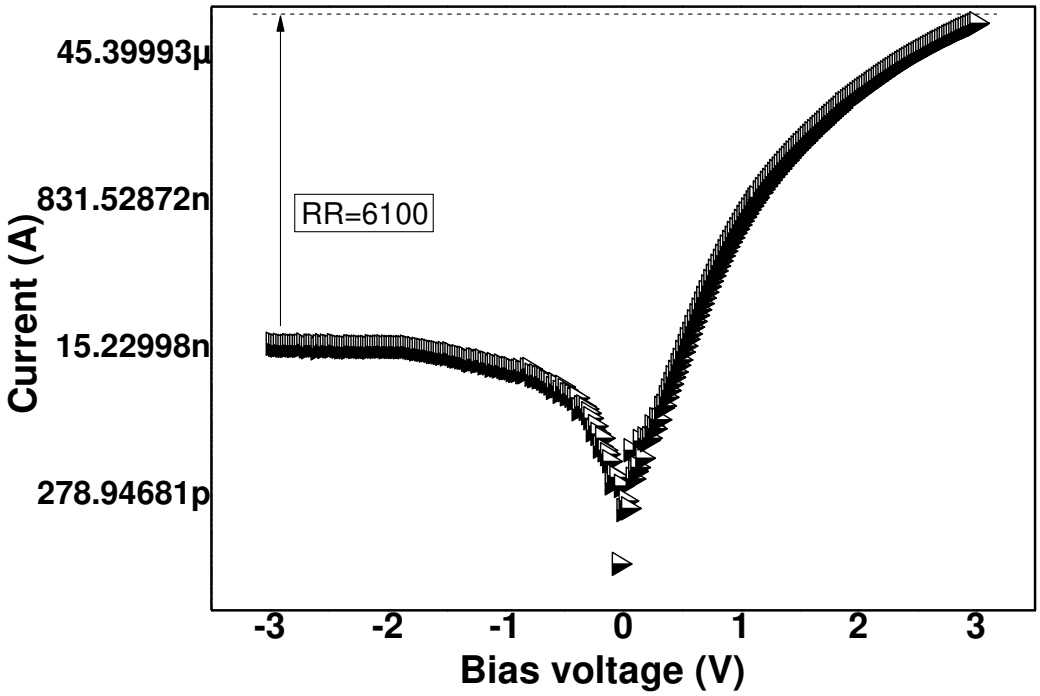

Fig.12b. Current-voltage characteristics of Au/ZnPc/pSi/Al produced by thermal evaporation route. Arrow indicates the rectification ratio (RR) of such organic diode.

Table 1: Selected the main functionals bond lengths and bond angles in the Pc molecule and Zn-Pc cluster

Bond lengths (Å)	Pc molecule	Zn-Pc cluster	Δ (%)
N2-N6	4.08662	3.98110	2.58
N4-N8	4.08662	3.98114	2.58
N2-C	1.39579	1.37315	1.62
N2=C	1.30082	1.37307	5.26
N4-C	1.39572	1.37310	1.62
N4=C	1.30085	1.37309	5.26
N6-C	1.39575	1.37313	1.62
N6=C	1.30084	1.37307	5.26
N8-C	1.39582	1.37311	1.62
N8=C	1.30081	1.37309	5.26
Bond angles (º)			
C-N1=C	120.22187	124.33138	3.30
C-N2=C	106.80056	109.40798	2.38
C-N3=C	120.22471	124.33593	3.30
C-N4=C	106.80303	109.40797	2.38
C-N5=C	120.22216	124.33488	3.30
C-N6=C	106.80347	109.40903	2.38
C-N7=C	120.22086	124.33286	3.30
C-N8=C	106.80101	109.40883	2.38

Table 2: Vibrational assignments, experimental and calculated wavenumbers (cm^{-1}) of Zn-Pc cluster and Pc molecule.

ZnPc (Experience)	ZnPc (DFT)	Pc (DFT)	Assignments
-	-	1720	ν(C=N) bending
-	-	1665	ν(C=C) bending
1508	1528	1480	ν_{as}(C-N-C) stretching
1447-1431	1429	-	ν_{s}(C-N-C) stretching
1338	1338	1369	ν(C-N-C) deformation
1302	1292	1274	ν(C-H) bending
1216	-	1209	ν_{as}(C- N(2,4,6,8)-C) stretching
1139	1164	1092	ν_{s}(C-N(2,4,6,8)-C) stretching
1106	1124	-	ν(N-Zn-N) rocking
944	996	1013	Benzene ring deformation
746	736	760	ν(N4-Zn-N8) deformation
675	665	671	ν(C-N-C) in pyrrole ring deformation
481	483	472	ν(N2-Zn-N6) deformation

Table 3: Calculated absorption wavelengths, energies, and oscillator strengths of Zn-Pc, and Pc molecule using TDDFT/B3LYP/6-31G(d,p)

Compounds	λ_{max} (nm)	Transition Energy (eV)	Oscillator strength
Zn-Pc	588	2.11	0.4596
	315	3.93	0.0683
	300	4.13	1.1492
	279	4.44	0.0777
	269	4.61	0.1151
	258	4.80	0.0156
Pc	388	3.19	0.0863
	348	3.56	0.0698
	318	3.90	0.0842
	295	4.20	0.3848
	279	4.44	0.0605
	244	5.08	0.0372

Table 4: The values of calculated dipole moment, polarizability, and second-order static hyperpolarizability of Zn-Pc, and Pc compounds.

Compounds	μ_{tot} (D)	α_{tot} $(10^{-24} esu)$	$\langle\gamma\rangle$ $(10^{-36} esu)$	Bandgap ΔE (eV)
Zn-Pc	0.0055	32.17	4.73	3.80
Pc	0.0033	28.31	4.34	5.13